The submitted manuscript has been authored by a contractor of the U.S. Government under Contract No. DE-AC05-96OR22464. Accordingly, the U.S. Government retains a nonexclusive royalty-free license to publish or reproduce the published form of this contribution, or allow others to do so, for U.S. Government purposes.

On the applicability of local asymptotic stability criteria to stellarator stability

B. A. Carreras and V. E. Lynch
Oak Ridge National Laboratory, Oak Ridge, Tennessee 37831, U.S.A
K. Ichiguchi
National Institute for Fusion Science, Toki, Japan.
M. Wakatani
Graduate School of Energy Science, Kyoto University, Kyoto, Japan
T. Tatsuno
Tokyo University, Tokyo, Japan

Abstract

An intrinsic consequence of the three-dimensional nature of the stellarator equilibrium may be the existence of local flattening of the pressure profile at the resonant surfaces. This local flattening of the pressure profile significantly changes the stability properties. The localized interchange modes are stabilized, and a new instability branch controls the critical beta. This instability is strongly stabilized by shear at high poloidal mode numbers. As a consequence, the plasma stability properties change, and the asymptotically derived local stability criteria often used in stellarator design are no longer applicable.

PACs: 52.55.Hc, 52.65.Kj, 52.35.-g

---

* Research sponsored by the Office of Fusion Energy, U.S. Department of Energy, under contract DE-AC05-00OR22725 with UT-Battelle, LLC

I. INTRODUCTION

Theoretically, ideal interchange modes should play a role in limiting the accessible beta (β) values in stellarators. This instability is particularly important for stellarators with a magnetic hill in the outer plasma region, such as the torsatron and heliotron configurations. In these configurations, low-*n* interchange instabilities may be defining the operational range of the device.[1] The Mercier criterion[2] gives a good estimate of the stability boundaries of both high-*n* and low-*n* ideal interchange modes.[3] However, it has been found that the limits given by the Mercier criterion are violated in some experiments.[4] To explain this disagreement, it may be argued that finite Larmour radius and/or kinetic effects probably stabilize the high-*n* modes. However, the issue of the stability of the low-*n* interchange modes remains.

To understand the cause of the discrepancy between theory and experiment, we turn our attention to the pressure profiles used in the estimates of stellarator stability. There are many reasons to suspect that pressure profiles with zero gradient at the rational surfaces may be the relevant profiles for stellarators. The existence of a three-dimensional (3-D) toroidal equilibrium is still an unresolved mathematical problem.[5] Of course, numerical solutions of the equilibrium magnetohydrodynamic (MHD) equations are commonly calculated. However, these solutions may just be weak solutions of these equations.[6] If the 3-D equilibrium exists, it may have magnetic structures (magnetic islands and/or stochastic regions) around the rational surfaces that increase transport in those regions; this increased transport will naturally lead to a local decrease of the pressure gradient. Other arguments can be made for such a pressure profile. From the perspective of having smooth particle fluxes in a 3-D equilibrium, Boozer[7] suggested that the pressure-gradient should be zero at the singular surfaces. In contrast, in dynamical calculations of equilibria unstable to resistive interchanges, we have seen the formation of flat spots at the resonant surfaces even for very low values of beta. In those calculations, we have observed a delicate interplay between resistive and ideal interchange modes. The first causes the local flattening of the pressure profile, which causes a modification of the stability threshold for the ideal modes. Finally, in experiment, high-resolution electron temperature and density measurements in TJ–II[8]

show the existence of multiple structures that may be related to the resonant surfaces. Therefore, it is reasonable to assume that the pressure profiles in stellarators have a complex structure with zero-gradient at each rational surface. The size of these flat spots can be very small, but even in such cases their presence has important consequences for stellarator stability.

In this paper, we pursue this idea further and investigate the linear stability of ideal interchange modes in the cylindrical geometry for plasmas with zero pressure gradient at the resonant surfaces. An analytical expression of the linear growth rate is derived and compared to numerical results. From these analytical results, we show that the β limits may be substantially increased over the estimates made with asymptotic local criteria evaluated with smooth pressure profiles.

The rest of the paper is organized as follows. In Sec. II, we introduce the equations used in the linear stability studies. The linear stability theory for pressure profiles with local flattening at the resonance surfaces is discussed in Sec. III. In Sec. IV, we discuss the effect of magnetic shear on these instabilities. The implications of these results for the asymptotic stability criteria are presented in Sec. V. Finally, the conclusions of this paper are given in Sec. VI.

II. STABILITY MODEL

Interchange modes, resistive and ideal, extend uniformly along the magnetic field lines. They are flutelike instabilities. Therefore, for these instabilities it is possible to average over the toroidal magnetic field modulation induced by the helical windings. Using the Greene and Johnson formalism[9] and assuming a straight helical system, the averaged equilibrium magnetic field geometry has cylindrical symmetry. In this system, the magnetic field line curvature is given by the averaged magnetic field line curvature,

$$\kappa \equiv \frac{d\Omega}{dr} = \frac{r}{R_0} B_0^2 V'' , \tag{1}$$

where prime indicates the derivative with respect to the toroidal flux, and $V' = \int d\ell / B$ is the specific volume enclosed by a flux surface. In Eq. (1), R_0 is the major radius of the stellarator, r the averaged minor radius of a flux surface, and B_0 the toroidal magnetic field at the magnetic axis.

We use a reduced set of MHD equations to describe the ideal interchange stability properties. The geometry is cylindrical with minor radius a and length $L_0 = 2\pi R_0$, and the cylindrical coordinates are r, θ,and z. The reduced set of MHD equations consists of the poloidal magnetic flux evolution equation,

$$\frac{\partial \psi}{\partial t} = -R_0 \quad {}_{\parallel} \Phi; \tag{2}$$

the perpendicular momentum balance equation,

$$\rho_m \frac{\partial \tilde{U}}{\partial t} = -\rho_m \vec{V} \qquad \tilde{U} - \quad {}_{\parallel} J_{\parallel} + \vec{z} \left(\vec{\Omega} \times \vec{P} \right); \tag{3}$$

and the equation of state,

$$\frac{\partial \tilde{p}}{\partial t} = -\tilde{\vec{V}} \qquad \tilde{p} - \frac{dp_{eq}}{dr} \tilde{V}_r + D \quad {}^2 \tilde{p} . \tag{4}$$

Here, p is the pressure, $\vec{V}$ is the perpendicular flow velocity, U is the z-component of the vorticity, ψ is the poloidal magnetic flux function, and ρ_m is the mass density. The total magnetic field can be expressed in terms of the poloidal flux function as

$$\vec{B} = -\left(\psi \times \hat{z} \right) / R_0 + B_0 \hat{z}; \tag{5}$$

and the perpendicular flow velocity can be expressed in terms of a stream function Φ/B_0 as

$$\vec{V} = \left(\Phi \times \hat{z} \right) / B_0 . \tag{6}$$

Here, $\hat{z}$ is the unit vector in the toroidal direction. The z-component of the vorticity can be expressed in terms of the velocity stream function by $\tilde{U} = {}^2\tilde{\Phi}$. The parallel derivative to the magnetic field, ${}_{\|}$, is defined as ${}_{\|} f = \vec{B} \quad f$.

In Eqs. (2)–(4), a tilde identifies perturbed quantities, and the subindex *eq* identifies equilibrium quantities. For the linear stability calculations presented here, each equation has been linearized in the perturbed quantities.

The driving term of the interchange instability is the pressure gradient in the bad curvature region ($\kappa > 0$). That is, these modes are driven by $-\kappa\left(dp_{eq}/dr\right) > 0$. The second term on the right-hand side of Eq. (2) is the field-line bending term, which is responsible for the magnetic shear stabilization effect.

For the numerical calculations, we use the averaged curvature of a helically symmetric system,

$$\frac{d\Omega}{dr} = \varepsilon^2 M\left(4r\iota + r^2\iota'\right) \quad . \tag{7}$$

Here, ε is the inverse aspect ratio, M is the number of toroidal field periods, and ι is the rotational transform. In calculating the stability properties, we use the linearized form of

Eqs. (2)–(4) and calculate the linear growth rate at different β values. The threshold β is obtained by extrapolating to a zero linear growth rate. In all calculations presented here, we have chosen a configuration with $M = 20$ and $\varepsilon = 0.1$.

III. LINEAR STABILITY PROPERTIES OF LOW-*N* INTERCHANGE MODES FOR PRESSURE PROFILES WITH ZERO GRADIENT AT THE SINGULAR SURFACES

In studying the stability properties of the pressure profiles with zero gradient at the rational surfaces, we begin considering a smooth pressure profile. For a smooth pressure profile, like $p_0(r) = \bar{p}_0\left(1 - r^2\right)$, the linear growth rate of an interchange mode as a function of β has been plotted in Fig. 1 (continuous line). For this instability the eigenfunction is sharply localized at and symmetric with respect to the singular surfaces (Fig. 2).

To investigate the changes in the stability properties when we consider a pressure profile, $p(r)$, which is like $p_0(r)$ but with zero gradient at the resonant surfaces, we modify the pressure profile in the following way:

$$p\,(r) = p_0(r) - \sum_m \left(dp/dr\right)\Big|_{r=r_m} \left[\left(r^2 - r_m^2\right)/\left(2r_m\right)\right] \exp\left[-\frac{\left(r - r_m\right)^2}{2W_m^2}\right], \tag{8}$$

where W_m is a measure of the size of the flat spot. The index m refers to the different resonant surfaces considered in the calculation. In studying the linear stability properties, we can start with one singular surface. For the rotational transform profile considered, we will carry out most of the calculations at the ι = 0.5 surface located at the radius $r_s = 0.497$.

Even for very small values of W_m, there is a qualitative change of the stability properties. For instance, Fig. 1 shows the linear growth of the instability (broken line) after modifying the pressure profile as described by Eq. (8) with $W_m/a = 0.004$. The result is that the instability threshold has increased by more than 60%, and the form of the eigenfunction has changed. The localized interchange instability branch (Fig. 2) is stable, and two other types of modes are now the fastest growing modes (Fig. 3). Their eigenfunctions are mirror-symmetric with respect the resonant surface, which is the one with the largest growth rate depends on details of the profiles and the exact location of

the flattening. Some of these changes in the stability properties of cylindrical plasmas have already been discussed elsewhere.[10-13] Here we will derive an analytic form for the dispersion relation and test the analytical results with numerical calculations. In Fig. 1, the linear stability results are for the (m = 6; n = 3) mode. The lower-m (m < 3) radially symmetric interchange modes may require a larger flat spot for full stabilization.[10] Note that the modification of the pressure profile by local flat spots with a width of $W_m/a = 0.004$ is hardly noticeable. For instance, Fig. 4 shows a parabolic pressure profile modified in the way indicated by Eq. (8) at the 15 lowest rational surfaces. Such a modification of the profile would require very high-resolution diagnostics to be detected in an experiment. Of course, in reality W_{m} may be larger than 0.004, and such detection may be possible. Low aspect ratio devices may be the most suitable ones for these experiment. The linear stability calculations also require very high resolution, here, we have used a radial grid of $\Delta r/a = 4 \times 10^{-5}$.

To understand the changes on stability properties, we will derive an analytic form for the dispersion relation of this new instability branch under some simplifying assumptions. From the set of reduced MHD equations, one can derive the eigenfunction equation for a mode (m; n):

$$\frac{d^2\Phi}{dr^2} + \left[\frac{1}{r} - \frac{2m\iota'(n-m\iota)}{\gamma^2+(n-m\iota)^2}\right]\frac{d\Phi}{dr} - \left[\frac{m^2}{r^2} + \frac{1}{\gamma^2+(n-m\iota)^2} \times \left(\frac{m\iota'}{r} + m\iota''(n-m\iota) - \frac{D_s m^2}{r^2}\right)\right]\Phi = 0 \quad . \tag{9}$$

Here, γ is the linear growth rate of the (m; n) mode and the eigenvalue for this problem, and D_s is

$$D_s = -\frac{\beta_0}{2\varepsilon^2}\frac{dp}{dr}\frac{d\Omega}{dr} \quad ,$$

with $\beta_0 = 2\mu_0 p(0)/B^2$.

An analytical solution for the linear stability problem for a pressure profile with zero gradient at the resonant surface can be found by dividing the minor radius in three regions as shown in Fig. 5. First we consider the case in which the eigenfunction is zero in the outer region of the radius (Fig. 3, broken line). One region is between the magnetic axis and $r_s - W/2$, where r_s is the radial position of the singular surface. In this region, we assume a constant rotational transform, ι_0, and parabolic pressure profile. A second region of width W is centered at the singular surface, and we assume that the profiles have zero pressure gradient and small magnetic shear. In the outer region, the values of the parameters do not matter because the eigenfunction is taken to be zero, $\Phi_{III}(r) = 0$.

In region I, the eigenfunction equation, Eq. (9), simplifies to

$$\frac{d^2\Phi}{dr^2} + \frac{1}{r}\frac{d\Phi}{dr} + \frac{m^2}{r^2}\left[\frac{D_s}{\gamma^2 + (n - m\iota)^2} - 1\right]\Phi = 0 \tag{10}$$

For the smooth pressure profile $p_0(r) = \bar{p}_0\left[1 - (r/r_0)^2\right]$, we have $D_s = (r/r_0)^2 \hat{D}_s$ with $\hat{D}_s = 4\beta_0 M\iota(0)$. In this case, Eq. (10) can be transformed into a Bessel equation, and the solution in region I verifying the origin boundary condition is

$$\Phi_I(r) = \lambda_1 J_m(\mu r) \ , \tag{11}$$

with

$$\mu^2 = \frac{m^2}{r_0^2}\frac{\hat{D}_s}{\gamma^2 + (n - m\iota_0)^2} \ . \tag{12}$$

In region II, the eigenvalue problem near the marginal point reduces to the Rosenbluth, Dagazian, and Rutherford solution[14] for the internal kink mode.

$$\Phi_{II}(r) = \lambda_2 \frac{r}{2}\left[1 - \frac{2}{\pi} ar\tan\left[\frac{m\iota'}{\gamma}\Big|(r - r_s)\right]\right] \quad . \tag{13}$$

For $r >> r_s$, $\Phi_{II} \approx 0$, and the solution in region II matches the outer region solution. For $W >> \gamma/m|\iota'|$, $\Phi_{II} \to \lambda_2 r$. In this case, we can match this asymptotic form to the inner region solution. From this match, we obtain a simple eigenvalue condition

$$\mu(r_s - W/2) = z_{ms} \quad . \tag{14}$$

From the eigenvalue condition, we can obtain the dispersion relation:

$$\gamma^2 = m^2\left[\frac{r_s - W/2}{r_0 z_{ms}} \hat{D}_s - \left(\frac{n}{m} - \iota_0\right)^2\right] \tag{15}$$

Here, z_{ms} is the *s*-zero of the function $F_m(z) \equiv zJ'_m(z) - J_m(z)$. For large *m*, $z_{ms} \approx j'_{ms}$, where j'_{ms} is the *s*-zero of the derivative of the J_m Bessel function of order *m*. Note that j'_{ms} scales as $m + 0.81m^{1/3}$ for large *m*. Because the first zero gives the highest growth rate, we will only consider this zero in what follows.

For small values of the flattening region *W*, we cannot take $\Phi_{II} \approx \lambda_2 r$. We have to use the full expression in Eq. (14). In this case, the eigenvalue condition is obtained from the solution of a transcendental equation. This implies that we still have Eq. (15) for the linear growth rate but substitute z_{ms} for $\hat{z}_m$, where $\hat{z}_m$ is a weak function of beta.

If the deviation from the z_{m1} value, $\Delta z = \hat{z}_m - z_{m1}$, is small, we can estimate the correction by linearizing the transcendental equation in Δz. We obtained

$$\Delta z = \frac{Az_{m1}\sqrt{B - z_{m1}^2}}{A\left(4B - 5z_{m1}^2\right)/\sqrt{B - z_{m1}^2} - \left(1 + z_{m1}^2 - m^2\right)/z_{m1}} \quad , \tag{16}$$

where

$$A = \frac{2}{W\pi} \frac{\left(m\iota_0 - n\right)^2}{\hat{D}_s\left(r_s - W/2\right)} \left[\frac{r_0}{m}\right]^2 \quad \text{and} \quad B = \left(\frac{m}{r_0}\right)^2 \frac{\left(r_s - W/2\right)^2}{\left(m\iota_0 - n\right)^2} \hat{D}_s \tag{17}$$

To test the analytical results, we have used a rotational transform profile of the form shown in Fig. 5. The rotational transform is $\iota = 0.32\left(1 + 2.2r^2 - 0.46r^4 + 2.5r^6\right)$ for $r \geq r_s - W/2$ and constant for $r \leq r_s - W/2$. Therefore, this profile is completely flat in the inner region of the plasma. The pressure profile used is parabolic with a flat region at the ι = 0.5 resonance surface.

When the size of the flat spot is very small, of the order of 1% of the radius, we have to solve the full transcendental equation obtained from the matching condition to get a good agreement between the analytical and numerical results. The result is illustrated in Fig. 6 for the (m = 6; n = 3) mode and different values of the width of the flat spot.

For a width of the order of 10% of the minor radius, we can use directly the dispersion relation Eq. (15) with the correction Δz calculated by Eq. (17). In this situation we get good agreement with the numerical results again. Figure 7 shows the linear growth rate of the (m = 6; n = 3) for W= 0.1 a as a function of beta and is compared with the dispersion relation, Eq. (15), with and without the correction Δz.

Equation (15) indicates that at a constant beta, the linear growth rate is strongly stabilized by flattening the pressure profile. Relatively small values of W/a can cause full stabilization of these modes,

$$W = 2\left[r_s - \frac{r_0 z_{m1} \left|\iota_0 - n/m\right|}{\hat{D}_s^{1/2}}\right] . \tag{18}$$

A similar analysis can be followed to find the solution, which is zero in the inner radial region. However, in this case using the constant ι approximation in the outer region of the plasma is less credible. Therefore, we will limit our study to the branch with zero eigenfunction in the outer region of the plasma.

IV. EFFECT OF MAGNETIC SHEAR IN THE STABILITY RESULTS

The analytical calculations show that near the stability threshold, the linear growth rate goes to zero by cancellation between the two terms in the r.h.s. of Eq. (15), the pressure gradient drive and the shear stabilizing term. Therefore, its value is very sensitive to the value of each of these two terms. In general, Eq. (15) can be used as guidance for the behavior of the growth rate, but it cannot be used as a quantitative measure of the growth rate in the case of a rotational transform profile with shear. Even in a case of a very low shear profile, the interpretation of the linear growth rate on the bases of the analytical is difficult. It is difficult to know what is the proper value to use for ι_0 when we compare with the numerical results for a realistic ι profile with shear.

Let us consider the ι = 0.5 resonant surface for the rotational transform profile $\iota = 0.32\left(1 + 2.2r^2 - 0.46r^4 + 2.5r^6\right)$. This is the same equilibrium considered before but without the flattening of the rotational transform profile in the inner region. The change of transform is small because the shear in the inner region is about 1. However, there are significant changes in the stability properties. The beta critical increases due to the shear stabilization effect [second term in the right-hand-side of Eq. (15)]. In Fig. 8, the linear growth rate vs beta for different modes and with W = 0.004 is plotted. The linear growth rate squared is no longer a linear function of beta. The reason for this change is that the type of instabilities discussed in the previous section is only relevant near the threshold. As beta increases, the modes broaden and become global modes (Fig. 9), and the dispersion relation Eq. (15) is not applicable to these modes. However, the important issue is that the instability threshold is still controlled by the same type of instability we just discussed.

Also with magnetic shear, by increasing W, one can achieve total stabilization of the pressure-driven modes. In Fig. 10, this effect is shown for the (m = 6; n = 3) and for several beta values. The size of W required increases with beta as indicated by Eq. (18).

The changes in the stability properties for the pressure profiles with flat spots at the resonant surfaces are not limited to cylindrical geometry. The averaging method has

been also used to study the stability properties of a realistic stellarator configuration with pressure profiles with zero gradient at the resonant surfaces. Once the toroidal couplings are also included in the model, one obtains similar changes in the stability properties.[12-15]

V. ASYMPTOTIC BEHAVIOR AND BETA CRITICAL

In looking for the asymptotic behavior of the linear growth rate with *m*, we can see from Eq. (15) that the growth rate dependence with *m* is quite different from the dependence of the local ideal interchange instability. For the latter, the linear growth rate is very weakly dependent on *m*. However, in the case of pressure profiles with local flattenings, the high *m* modes are strongly suppressed. In Fig. 11 and for the same equilibrium parameters as the cases in Fig. 8, we show the linear growth as a function of *m*. These calculations have been done with $W = 0.004\,a$. In Fig. 11, we can see the decrease in the growth rates with increasing *m* and the total stabilization of the high-*m* modes. They are contrasted with the behavior of the linear growth rate in case of a smooth profile with $W = 0$. Hence, the large *m* asymptotic stability criteria cannot have any information on the stability of the modes described by Eq. (15). Furthermore, those criteria became undefined in the case of a zero pressure gradient in each rational surface. Therefore, for those pressure profiles the asymptotic local stability criteria cannot be applied.

From Eq. (15) we can calculate the corresponding critical beta for these new instabilities. For fixed *W*, the critical beta value scales as m^2 because $z_{m1} \quad m$. Therefore, the beta critical at a given surface is given by the beta critical for the lowest *m* value.

$$\beta_0^c = \frac{1}{4M\iota_0}\left(\frac{r_0 z_{m_0 1}}{r_s - W/2}\right)^2 \left(\frac{n}{m} - \iota_0\right)^2 . \tag{19}$$

Here m_0 is the lowest *m* value at the resonant surface considered. For an equilibrium with magnetic shear, the beta critical scales qualitatively in a similar way as the zero-shear case (Fig. 12). That is, increases with *m*. However, the scaling exponent is no longer 2, but somewhat smaller.

If we now take the smooth profile, $p_0(r)$, corresponding to the pressure profile with flat spots, $p(r)$, we can calculate the critical beta given by the Suydam criterion,

$$\beta_{0S}^{c} = \frac{\left(\iota_s' r_0\right)^2}{16 M \iota_0} \quad , \tag{20}$$

where we have taken $\iota_s' \equiv d\iota / dr\big|_{r=r_s}$. The form is similar to the one given by Eq. (19). We can compare the real beta critical, Eq. (19), with the Suydam beta critical, β_{0S}^{c}. If we take $\iota_0 \approx \iota\left(r_s\right) + r_s \iota_s'$, we obtain

$$\beta_0^c \approx \left(2 z_{m_0 1}\right)^2 \beta_{0S}^{c} . \tag{21}$$

We see that the real beta critical can be of order of magnitude higher than the critical beta from the Suydam criterion β_{0S}^{c} calculated with a smooth pressure profile.

Therefore, local stability criteria like the Suydam criterion calculated with a smooth pressure profile cannot be applied to configurations with a pressure profile with zero gradient at each rational surface. Such criteria may be used as a measure of stability if a convenient normalization constant can be found.

VI. CONCLUSIONS

For stellarator equilibrium with zero-pressure gradient at the rational surfaces local, asymptotic stability criteria cannot be applied. For stellarators, the Mercier criterion has the same problems as the Suydam criterion in cylindrical geometry. It is a local stability criterion that cannot be applied to such pressure profiles. Calculations using the averaged method approach indicate that the stability properties for the low-*m* modes[12-15] are similar to the case of cylindrical geometry. The local interchangelike modes are stabilized, and the more global type eigenfunction are the residual instabilities. The beta critical also increases over the one obtained for smooth pressure profiles. These results may explain the apparent violation of this criterion when smooth pressure profiles are used in calculation of the stability for interpretation of the experimental measurements.[4]

ACKNOWLEDGMENTS

This research was sponsored in part by Oak Ridge National Laboratory, managed by UT-Battelle, LLC, for the U.S. Department of Energy under contract number DE–AC05-00OR22725.

REFERENCES

[1]V. D. Shafranov, Phys. Fluids **26**, 357 (1983).

[2]C. Mercier, Nucl. Fusion **1**, 47 (1960).

[3]N. Dominguez, J. N. Leboeuf, B. A. Carreras, et al., Nuclear Fusion **29**, 2079 (1989).

[4]S. Okamura, K. Matsuoka, R. Akiyama, et al., Nucl. Fusion **39**, 1337 (1999).

[5]H. Grad, Phys. Fluids **7**, 1283 (1964).

[6]F. Bauer, O. Betancourt, and P. Garabedian, "Magnetohydrodynamic Equilibrium and Stability" Springer-Verlag, New York, 1984.

[7]A. H. Boozer, Phys. Fluids **24**, 1999 (1981).

[8]J. Herranz, I. Pastor, F. Castejón et al., Phys. Rev. Lett. **85**, 4715 (2000).

[9]J. M. Greene and J. L. Johnson, Phys. Fluids **4**, 875 (1961).

[10]B. A. Carreras, V. E. Lynch, K. Ichiguchi, T. Tatsuno, and M. Wakatani, Plasma Physics Reports **25**, 958 (1999).

[11]M. Wakatani, K. Ichiguchi, T. Tatsuno, M. Furukawa, B. A. Carreras, and V. E. Lynch, J. Plasma Fus. Res. **2**, 39 (1999).

[12]K. Ichiguchi, N. Nakajima, M. Okamoto, N. Ohyabu, T. Tatsuno, M. Wakatani, and B. A. Carreras, J. Plasma Fus. Res. **2**, 286 (1999).

[13]T. Tatsuno, M. Wakatani, and K. Ichiguchi, Nucl. Fusion 39, 1391 (1999).

[14]M. N. Rosenbluth, R. Y. Dagazian, and P. H. Rutherford, Phys. Fluids 16, 1894 (1973).

[15]K. Ichiguchi, M. Wakatani, T. Unemura, T. Tatsuno, and B. A. Carreras, Nucl. Fusion (in press).

FIGURE CAPTIONS

Fig.1 Linear growth rate of the (m = 6; n = 3) mode for an equilibrium with parabolic pressure profile and $\iota = 0.32\left(1 + 2.2r^2 - 0.46r^4 + 2.5r^6\right)$.

Fig. 2. Eigenfunctions for the m = 6 localized interchange mode for a smooth parabolic pressure profile.

Fig. 3. Eigenfunctions for the m = 6 mode for the most likely unstable modes once the localize interchange mode has been stabilized.

Fig. 4. Parabolic pressure profile modified in the way indicated by Eq. (8) at the 15 lowest rational surfaces.

Fig. 5. Pressure and rotational transform profile used in the analytical determination of the dispersion relation Eq. (15).

Fig. 6. Square of the linear growth rate of the (m = 6; n = 3) mode vs β for different values of W. Numerical results are compared to the analytical calculation. The equilibrium parameters are given in Fig. 5.

Fig. 7. Square of the linear growth rate of the (m = 6; n = 3) mode vs β for $W = 0.1\,a$. Numerical results are compared to the analytical calculation given by Eq. (15) with and without correction terms. The equilibrium parameters are given in Fig. 5.

Fig. 8. Linear growth rate of the (m = 2; n = 1), (m = 6; n = 3), and (m = 10; n = 5) modes as a function of β for an equilibrium with parabolic pressure profile with a flat spot of $W = 0.004\,a$ and $\iota = 0.32\left(1 + 2.2r^2 - 0.46r^4 + 2.5r^6\right)$.

Fig. 9. Eigenfunction of the (m = 6; n = 3) mode for different values of β. These results correspond to the same parameters used in Fig. 8.

Fig. 10. Linear growth rate of the (m = 6; n = 3) mode as a function of W for different values of β. These results correspond to the same parameters used in Fig. 8.

Fig. 11. Linear growth rate as a function of m for different values of β. These results correspond to the same parameters used in Fig. 8.

Fig. 12. β_c as a function of m for different values of W. These results correspond to the same parameters used in Fig. 8.

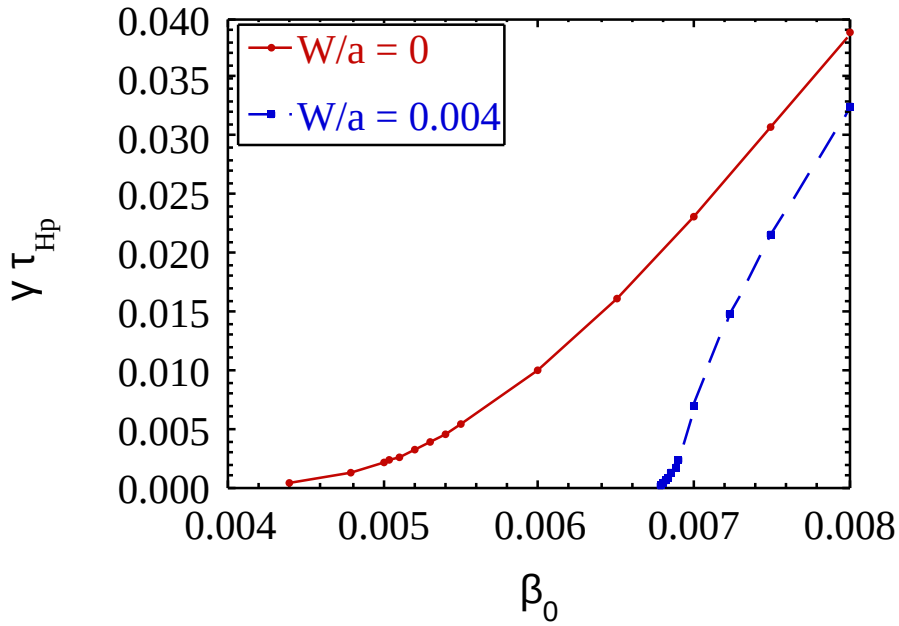
W/a = 0
W/a = 0.004
0.040
0.035
0.030
0.025
0.020
0.015
0.010
0.005
0.000
γ τ_Hp
0.004
0.005
0.006
0.007
0.008
β_0

Fig. 1

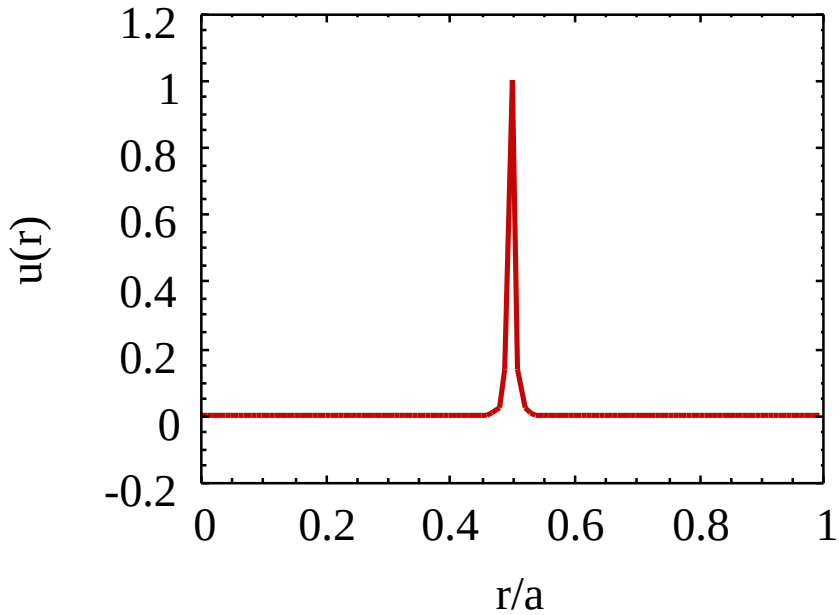
1.2
1
0.8
0.6
0.4
0.2
0
-0.2
u(r)
0
0.2
0.4
0.6
0.8
1
r/a

Fig. 2

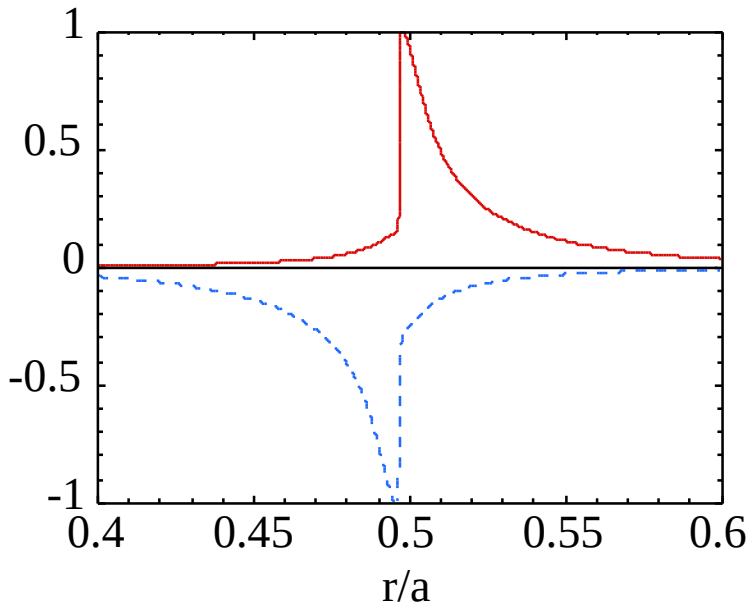

Fig. 3

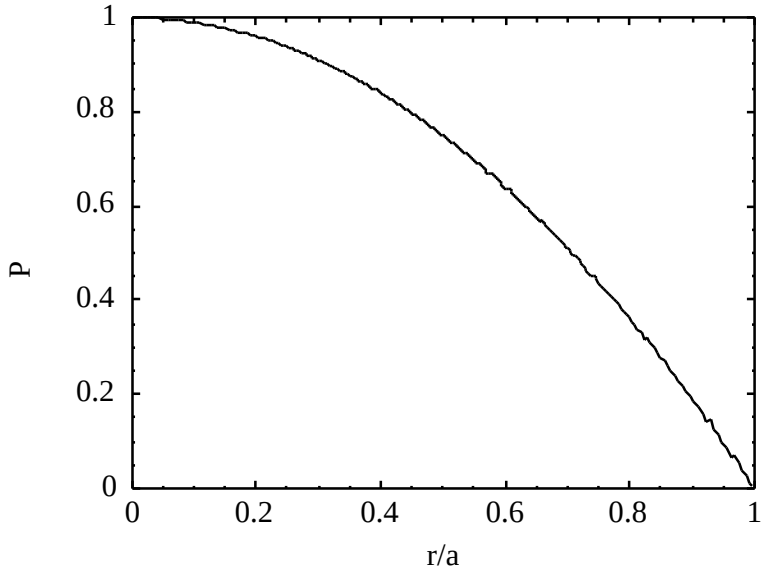

Fig. 4

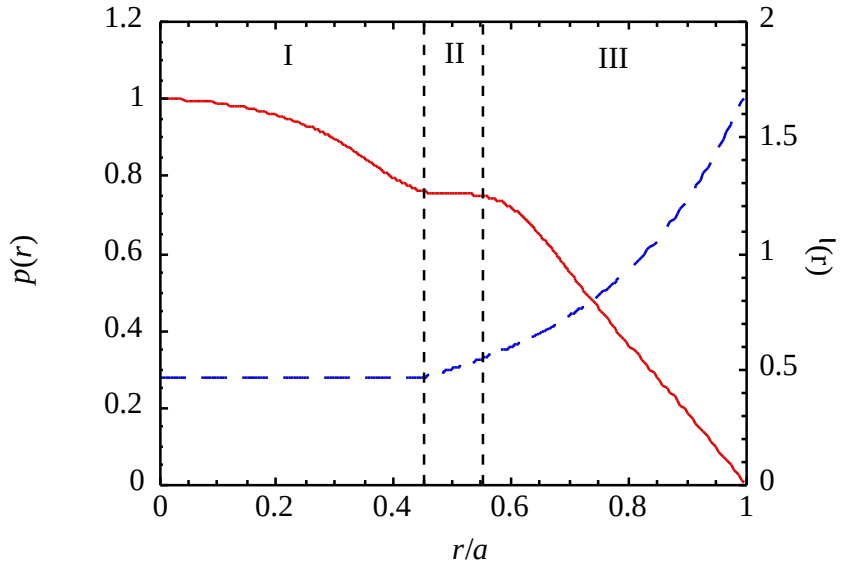
I
II
III
p(r)
l(r)
r/a
0
0.2
0.4
0.6
0.8
1
1.2
0.5
1.5
2

Fig. 5

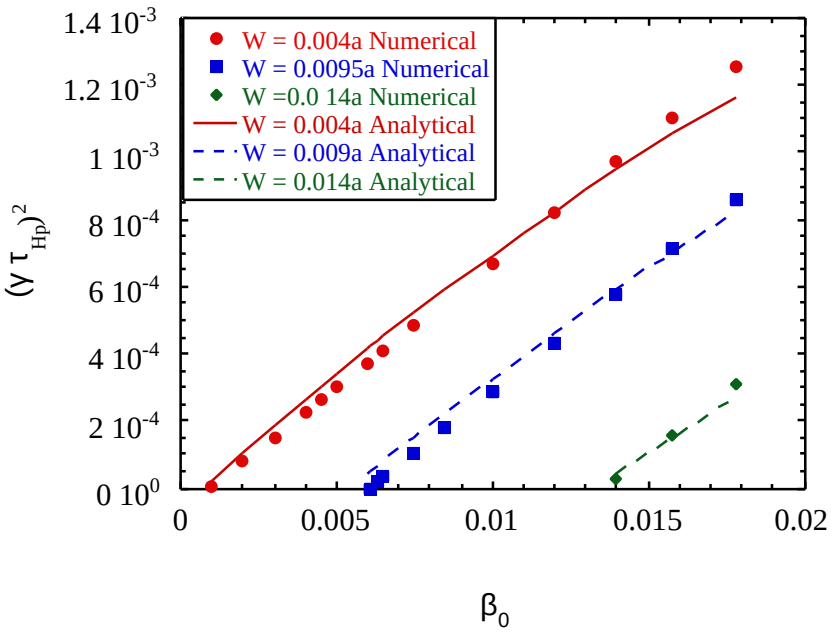
W = 0.004a Numerical
W = 0.0095a Numerical
W =0.0 14a Numerical
W = 0.004a Analytical
W = 0.009a Analytical
W = 0.014a Analytical
(γ τ_Hp)^2
β_0
0 10^0
2 10^-4
4 10^-4
6 10^-4
8 10^-4
1 10^-3
1.2 10^-3
1.4 10^-3
0
0.005
0.01
0.015
0.02

Fig. 6

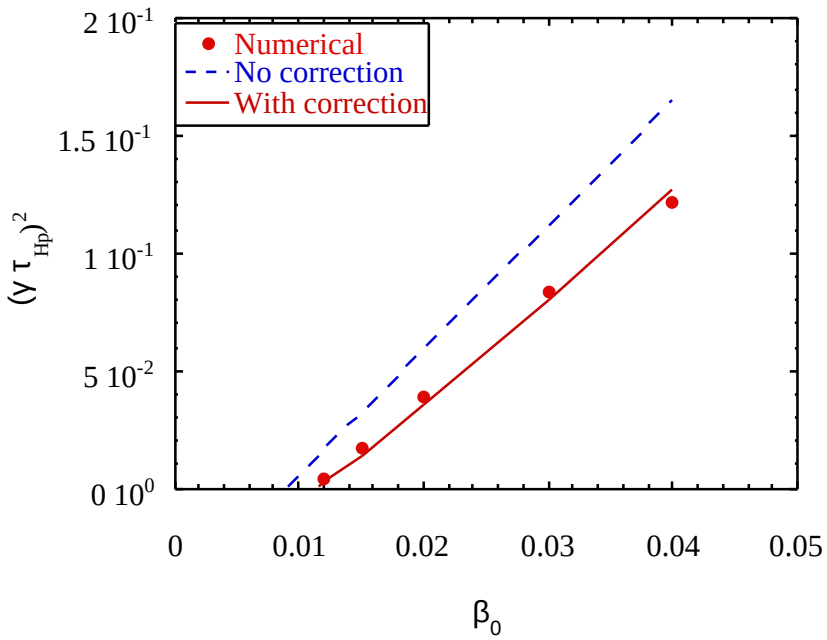
Numerical
No correction
With correction
2 10-1
1.5 10-1
1 10-1
5 10-2
0 100
(γ τHp)2
0
0.01
0.02
0.03
0.04
0.05
β0

Fig. 7

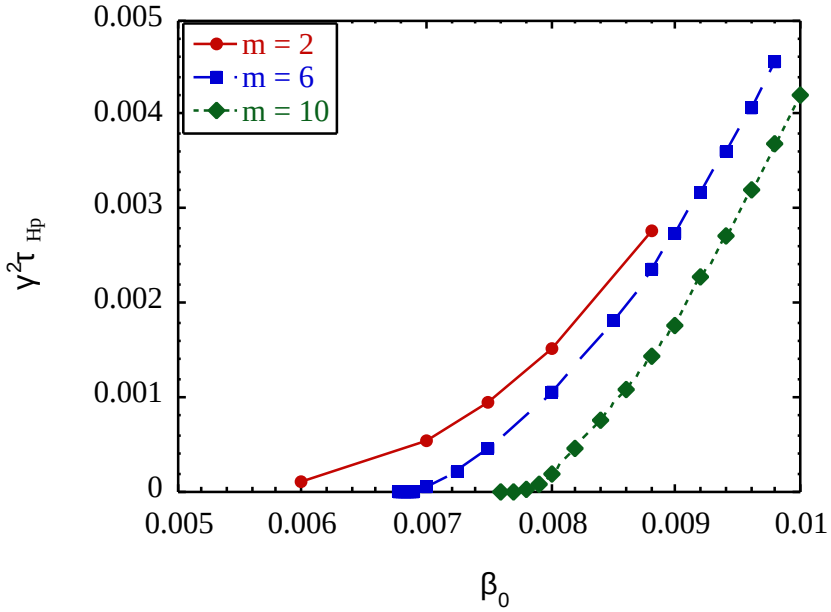
m = 2
m = 6
m = 10
0.005
0.004
0.003
0.002
0.001
0
γ2τ Hp
0.005
0.006
0.007
0.008
0.009
0.01
β0

Fig. 8

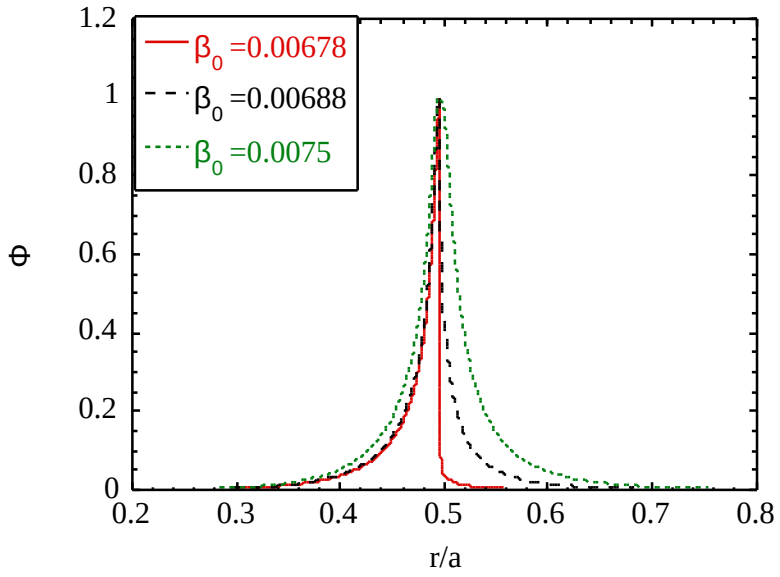
1.2
1
0.8
0.6
0.4
0.2
0
Φ
0.2
0.3
0.4
0.5
0.6
0.7
0.8
r/a
β0 =0.00678
β0 =0.00688
β0 =0.0075

Fig. 9

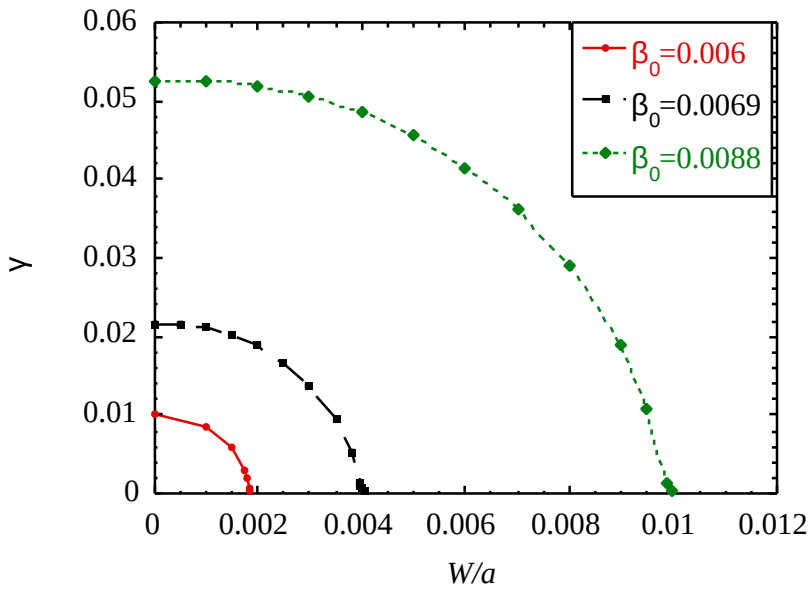
0.06
0.05
0.04
0.03
0.02
0.01
0
γ
0
0.002
0.004
0.006
0.008
0.01
0.012
W/a
β0=0.006
β0=0.0069
β0=0.0088

Fig. 10

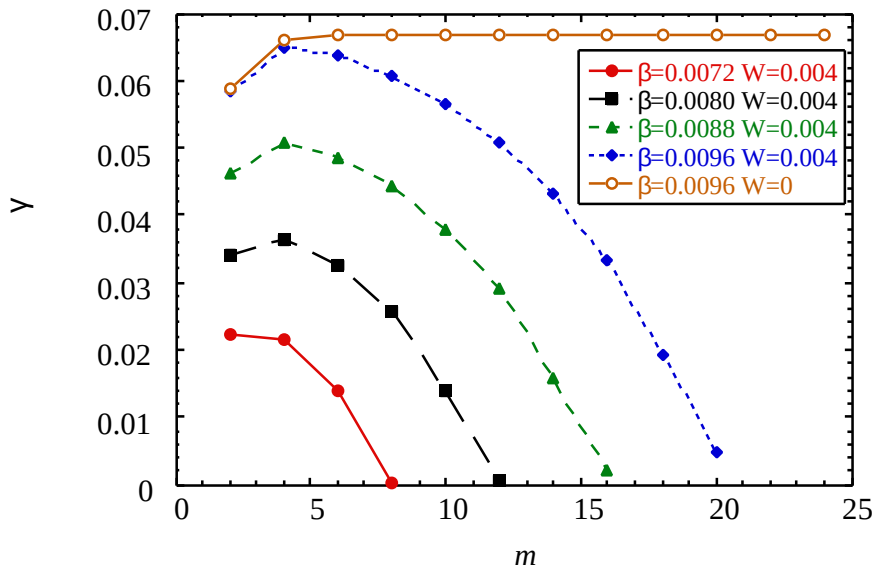
0.07
0.06
0.05
0.04
0.03
0.02
0.01
0
γ
0
5
10
15
20
25
m
β=0.0072 W=0.004
β=0.0080 W=0.004
β=0.0088 W=0.004
β=0.0096 W=0.004
β=0.0096 W=0

Fig. 11

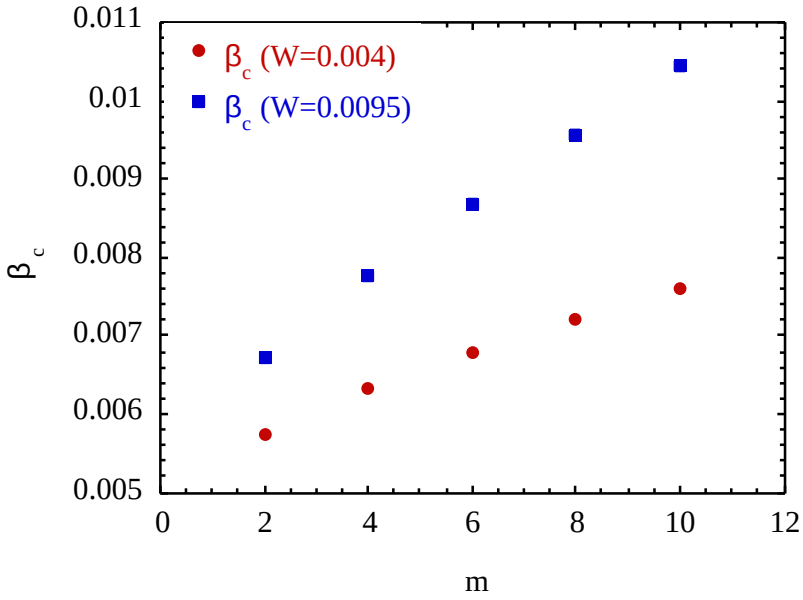
0.011
0.01
0.009
0.008
0.007
0.006
0.005
β c
0
2
4
6
8
10
12
m
β c (W=0.004)
β c (W=0.0095)

Fig. 12